Article

Dualities and non-Abelian mechanics

https://doi.org/10.1038/s41586-020-1932-6

Received: 26 April 2019

Accepted: 11 November 2019

Published online: 20 January 2020

Michel Fruchart[1,2]*, Yujie Zhou[3] & Vincenzo Vitelli[1,2]*

Dualities are mathematical mappings that reveal links between apparently unrelated systems in virtually every branch of physics[1–8]. Systems mapped onto themselves by a duality transformation are called self-dual and exhibit remarkable properties, as exemplified by the scale invariance of an Ising magnet at the critical point. Here we show how dualities can enhance the symmetries of a dynamical matrix (or Hamiltonian), enabling the design of metamaterials with emergent properties that escape a standard group theory analysis. As an illustration, we consider twisted kagome lattices[9–15], reconfigurable mechanical structures that change shape by means of a collapse mechanism[9]. We observe that pairs of distinct configurations along the mechanism exhibit the same vibrational spectrum and related elastic moduli. We show that these puzzling properties arise from a duality between pairs of configurations on either side of a mechanical critical point. The critical point corresponds to a self-dual structure with isotropic elasticity even in the absence of spatial symmetries and a twofold-degenerate spectrum over the entire Brillouin zone. The spectral degeneracy originates from a version of Kramers' theorem[16,17] in which fermionic time-reversal invariance is replaced by a hidden symmetry emerging at the self-dual point. The normal modes of the self-dual systems exhibit non-Abelian geometric phases[18,19] that affect the semiclassical propagation of wavepackets[20], leading to non-commuting mechanical responses. Our results hold promise for holonomic computation[21] and mechanical spintronics by allowing on-the-fly manipulation of synthetic spins carried by phonons.

Symmetries and their breaking govern natural phenomena from fundamental particles to molecular vibrations[22]. They are also powerful tools to design synthetic materials from chemical compounds to metamaterials[23–27]. Here we start by asking a question almost deceptive in its simplicity: what is a symmetry? A symmetry is a transformation that maps a system onto itself, as illustrated by the threefold rotation C_3 acting on the structure in Fig. 1a. A duality, on the other hand, relates distinct models or structures[1–8]. A celebrated example is the Kramers–Wannier order–disorder duality[1,2] between the low- and high-temperature phases of the two-dimensional Ising model, pictured in Fig. 1b. In self-dual systems, the distinction between dualities and symmetries is blurred: additional symmetries can emerge at a self-dual point even if the spatial symmetries are unchanged. This is what occurs in the critical configuration of the mechanical system shown in the middle panel of Fig. 1c. Here we show how such dualities can be harnessed to engineer material properties from wave propagation to static responses that are not predicted by a standard symmetry analysis based on space groups.

Mechanical structures are described at the linear level by normal modes of vibration and their oscillation frequencies. Both are determined by the dynamical matrix $\hat{D}$, which summarizes the Newton equations of motion in the harmonic approximation $\partial_t^2|\phi\rangle = -\hat{D}|\phi\rangle$. The vector $|\phi\rangle$ has components $\phi_p = u_p\sqrt{m_p}$, where u_p is the displacement of particle p with mass m_p from its equilibrium position. The eigenvectors $|\phi_i\rangle$ and eigenvalues ω_i^2 of the dynamical matrix, such that $\hat{D}|\phi_i\rangle = \omega_i^2|\phi_i\rangle$, are the normal modes of vibration and the corresponding angular frequencies. In a spatially periodic system, the spectrum of the Bloch dynamical matrix $D(k)$ is organized in frequency bands with dispersion relations $\omega_i(k)$ parameterized by quasi-momenta k forming the Brillouin zone of the crystal. Although our discussion is focused on mechanics, our analysis applies when $\hat{D}$ is replaced by other linear operators, such as the Maxwell operator of a photonic crystal[28], the mean-field Hamiltonian of a quantum system (in which case the eigenvalues are energies) or the dynamical matrix of an electrical circuit[29–31].

Twisted kagome lattices are a family of structures obtained from a mechanical kagome lattice[9–15] by actuating a mechanism, called a Guest–Hutchinson mode[9], that allows a global deformation of the unit cells (see Supplementary Video demonstrating this property). This family is parameterized by a twisting angle θ described in Fig. 2. We denote by $\hat{D}(\theta)$ the dynamical matrix of the structure with twisting angle θ. To each twisted kagome lattice with a twisting angle θ corresponds a dual mechanical structure, which is another twisted kagome lattice with a twisting angle $\theta^* = 2\theta_c - \theta$. Comparison of the lower panels of Fig. 2b, d reveals that two lattices related by a duality transformation share the same band structure despite their clear structural difference. Remarkably, there is a self-dual kagome structure with angle $\theta_c^* = \theta_c + \pi/4$, where the band structure is doubly degenerate over the entire Brillouin zone, as shown in the lower panel of Fig. 2c. We now prove that the explanation of these phenomenological observations can be traced to the existence of a mathematical duality between the dynamical matrices of pairs of kagome lattices. An application of our

[1]James Franck Institute, University of Chicago, Chicago, IL, USA. [2]Department of Physics, University of Chicago, Chicago, IL, USA. [3]Instituut-Lorentz, Universiteit Leiden, Leiden, The Netherlands. *e-mail: fruchart@uchicago.edu; vitelli@uchicago.edu

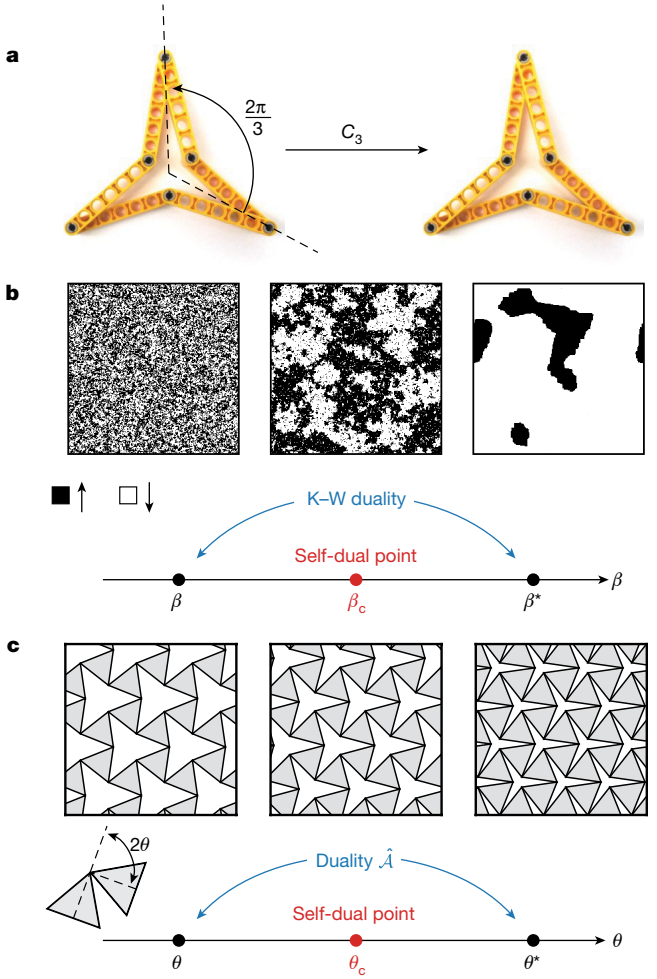

Fig. 1 | Symmetries and dualities. a, A star-shaped polygon in LEGO bricks illustrates threefold rotation symmetry: the mechanical molecule is mapped to itself by a 2π/3 (120°) rotation C_3. This is in contrast to a duality, which generically maps one system to another system. **b**, In the Ising model, spins on a two-dimensional lattice can take two values, ±1, represented by black (white) pixels. A phase transition separates an ordered ferromagnetic phase at low temperature in which spins align (right panel) from a disordered paramagnetic phase at high temperature (left panel). The Kramers and Wannier duality[1] associates to each (inverse) temperature β a dual temperature β^*, and the ratio of the partition functions at β and β^* is a known smooth function. The self-dual point $\beta_c = \beta_c^*$ corresponds to the critical phase (middle panel), where the phase transition between the ferromagnet and the paramagnet occurs. **c**, Twisted kagome lattices form a family of mechanical structures parameterized by a variable θ called the twisting angle. (See Fig. 2 for a model in LEGO bricks.) To each kagome lattice with angle θ is associated a dual kagome lattice with angle $\theta^* = 2\theta_c - \theta$, resulting in strong relations between their mechanical properties. At the self-dual point, where $\theta_c = \theta_c^* \equiv \pi/4$, the duality becomes a symmetry.

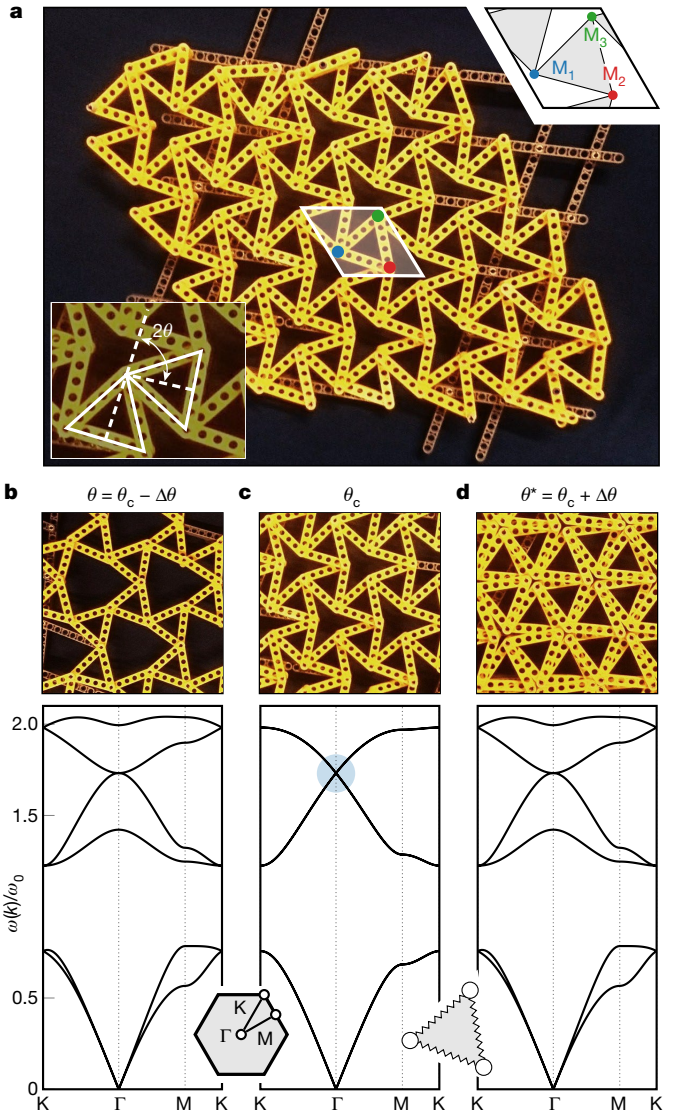

Fig. 2 | Twisted kagome lattices and their band structures. a, A LEGO bricks realization of the twisted kagome lattice tuned close to the critical point θ_c. Lower inset: visualization of the twisting angle θ. The angle between two triangles is $\pi - 2\theta$. Upper inset: unit cell of the mechanical structure. There are three inequivalent points (that is, not related by Bravais lattice translations) labelled M_1, M_2 and M_3. **b**–**d**, Band structures of the mechanical structures at different twisting angles. The physical frequencies are non-dimensionalized by a characteristic frequency, $\omega_0 = \sqrt{(k_0/m_0)}$, where k_0 and m_0 are the characteristic spring constant and the mass, respectively. The dual twisted kagome lattices with twisting angles $\theta_c \pm \Delta\theta$ have the same band structure (**b** and **d**). The self-dual lattice with twisting angle θ_c (**c**) has an twofold-degenerate band structure (including for points outside high-symmetry lines). At the Γ point, a double Dirac cone can be observed, highlighted by a blue shaded circle. The band structures are obtained by diagonalizing the Bloch dynamical matrices $D(\theta, k)$. The masses m_i of points M_i are set to unity in units of m_0. See Supplementary Information for details and a video demonstrating the collapse mechanism.

general approach to electrical circuits is outlined in the Supplementary Information.

We first introduce a unitary transformation $\hat{\mathcal{U}}$ acting on the vibrational degrees of freedom of a twisted kagome lattice as represented in Fig. 3. A direct calculation (see Supplementary Information) shows that

$$\mathcal{U}(k)D(\theta^*, -k)\mathcal{U}^{-1}(k) = D(\theta, k) \quad (1)$$

where $\mathcal{U}(k)$ is the Bloch representation of operator $\hat{\mathcal{U}}$. Hence, $\hat{\mathcal{U}}$ should be viewed as a linear map between different spaces, describing the vibrations of the different mechanical structures with twisting angles θ^* and θ (compare the two lattices in Fig. 3). Note that $\mathcal{U}(k)$ does not depend on the twisting angle θ. As Newton equations are real-valued, the Bloch dynamical matrix satisfies $\Theta D(\theta, k)\Theta^{-1} = D(\theta, -k)$ where Θ is complex conjugation. Hence, by combining the anti-unitary operator $\hat{\Theta}$ with $\hat{\mathcal{U}}$, we get an anti-unitary operator $\mathcal{A}(k) = \mathcal{U}(k)\Theta$, which squares to $\mathcal{A}(k)^2 = -\mathrm{Id}$ (where Id is the identity matrix) and such that

$$\mathcal{A}(k)D(\theta^*, k)\mathcal{A}^{-1}(k) = D(\theta, k) \quad (2)$$

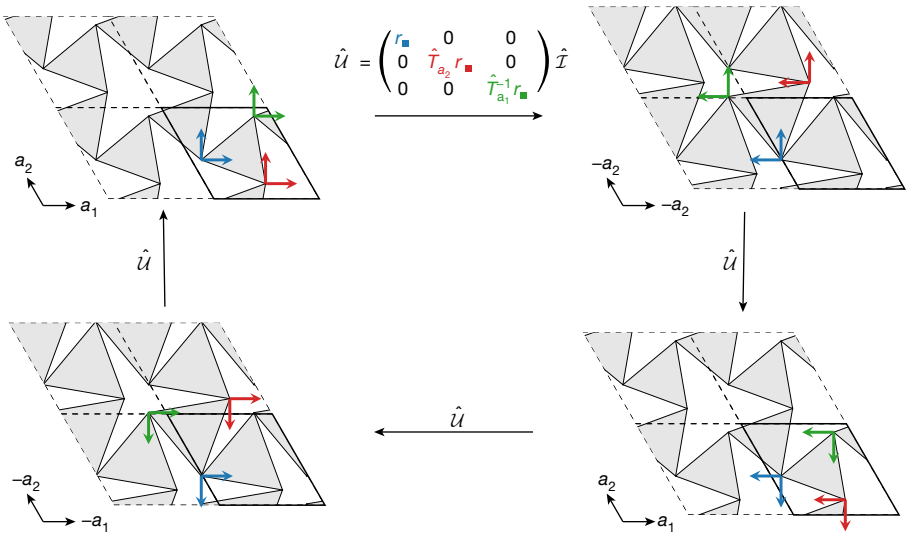

Fig. 3 | Schematic action of the duality operator. The duality operator maps the vibrational degrees of freedom of a twisted kagome lattice to the vibrational degrees of freedom of the dual kagome lattice. The vibrational degrees of freedom (in blue, red and green) in a unit cell (bold outline) are rotated by 90° counterclockwise and translated to another unit cell. Importantly, the translation depends on the degree of freedom: the vibrations of mass M_1 (in blue) are not shifted, whereas the vibrations of mass M_2 (in red) are shifted by one lattice vector a_2 and the vibrations of mass M_3 (in green) are shifted by another lattice vector $-a_1$. The operator $\hat{\mathcal{U}}$ is written as a block matrix; the different blocks describe the different masses in the unit cell (as represented by the colours), and the (real) matrices $r_{\blacksquare} \equiv \mathrm{i}\sigma_y$ (the square represents fourfold rotation on the degrees of freedom) act for each mass on the two orthogonal vibrations along x and y, mapping (u_x, u_y) to $(u_y, -u_x)$. The operator $\hat{\mathcal{I}}$ acts on the Bravais lattice as space inversion, but does not modify the internal degrees of freedom (see Supplementary Information). Iterated applications of $\hat{\mathcal{U}}$ show that $\hat{\mathcal{U}}^2 = -\mathrm{Id}$, $\hat{\mathcal{U}}^3 = -\hat{\mathcal{U}}$ and $\hat{\mathcal{U}}^4 = \mathrm{Id}$, showing that the symmetry has order 4. In the self-dual lattice, the transformation resembles a non-symmorphic symmetry composed of a 90° rotation followed by a non-integer lattice translation at first sight. However, further inspection shows that this operation is different from the duality operation, and is not a symmetry of the self-dual lattice (see Supplementary Information for a visual proof).

Equation (2) is the expression of a duality between the two lattices with twisting angles θ and θ^*, illustrated in Fig. 1c. The dynamical matrices of the two dual systems are related by a anti-unitary transformation. As a consequence, they have identical band structures (more precisely, the eigenvalues are related by complex conjugation, and are equal because they are also real) and the eigenvectors are related by $\mathcal{A}$. Equation (1) is also a duality between the same lattices. In contrast to equation (2), it is ruled by a unitary operator, but is non-local in momentum space (it relates k to $-k$). Alone, it would ensure that the band structures of both lattices are the same only up to an inversion of momentum.

We now move on to explain the global twofold degeneracy observed in Fig. 2c. This degeneracy is reminiscent of a celebrated theorem from Kramers[16,17] stating that the energy states of time-reversal invariant quantum systems with half-integer spin are at least doubly degenerate. At first sight, this theorem does not apply here, as the mechanical degrees of freedom are neither quantum mechanical nor fermionic. Yet Kramers' theorem can still formally apply provided that some anti-unitary operator squaring to minus the identity matrix commutes with the dynamical matrix. At the critical twisting angle $\theta_c = \theta_c^* \equiv \pi/4$, the mechanical structure is self-dual. The duality shown in equation (2) acts as a hidden symmetry of the critical dynamical matrix $D(\theta_c)$, through $\mathcal{A}(k)D(\theta_c, k)\mathcal{A}^{-1}(k) = D(\theta_c, k)$. As $\mathcal{A}^2 = -\mathrm{Id}$, Kramers' theorem can indeed be applied, and implies that the band structure is twofold degenerate at every point k of the Brillouin zone, as observed in Fig. 2c. Interestingly, $\mathcal{A}$ acts in the same way as the combination of spatial inversion and a so-called fermionic time-reversal would in an electronic system, although neither is present in our mechanical system. Owing to the presence of the self-dual symmetry, the critical band structure exhibits exotic features. For instance, a finite-frequency linear dispersion (a double Dirac cone) is observed at the centre of the Brillouin zone (called Γ; see Fig. 2c) that is uncommon in systems with time-reversal invariance (see Supplementary Information for a discussion and references).

When the self-duality is combined with the usual crystal symmetries, anomalous point groups can be realized. Consider paving the two-dimensional plane with a single regular polygon. This is possible with a triangle, a square or a hexagon, but not with a pentagon or a dodecagon. This is a manifestation of the crystallographic restriction theorem: the only point group symmetries compatible with lattice translations are of order 1, 2, 3, 4 or 6, in two dimensions. (The order of an operation g is the smallest integer n such that g^n is the identity matrix.) The point group C_{3v} of twisted kagome lattices at the centre Γ of the Brillouin zone contains threefold rotations (as visible in Fig. 2), perfectly compatible with this assertion. At the critical angle θ_c, the duality relation (1) turns into an additional symmetry of the dynamical matrix. The point group at Γ has effectively to be supplemented with $\mathcal{U}(\Gamma)$, which has order 4 (see Fig. 3). Combined with a threefold rotation from C_{3v}, the self-dual symmetry $\mathcal{U}(\Gamma)$ produces an anomalous symmetry of order $3 \times 4 = 12$, making the effective point group at Γ non-crystallographic (isomorphic to D_{12}; see Supplementary Information). The emergence of this non-crystallographic point group is curious, as the twisted kagome lattices are indeed crystals, not quasicrystals. However, there is no contradiction with the crystallographic restriction theorem, because the self-dual symmetry is not a spatial symmetry.

Besides vibrational modes, the duality induces a relation between the elastic tensors $c_{ijk\ell}(\theta)$ and $c_{ijk\ell}(\theta^*)$ that describe the static mechanical response of dual structures in the linear regime (see Supplementary Information). A striking manifestation of the enhanced symmetry at the self-dual point is revealed by considering the elastic tensors of a twisted kagome lattice in which inequivalent springs have different stiffnesses. In this case. there are no spatial symmetries besides translations (the space group is $p1$). In the Supplementary Information, we show that three distinct elastic moduli exist for $\theta \neq \theta_c$, whereas at the self-dual point $\theta = \theta_c$ the elastic tensor becomes isotropic and only one non-vanishing modulus remains.

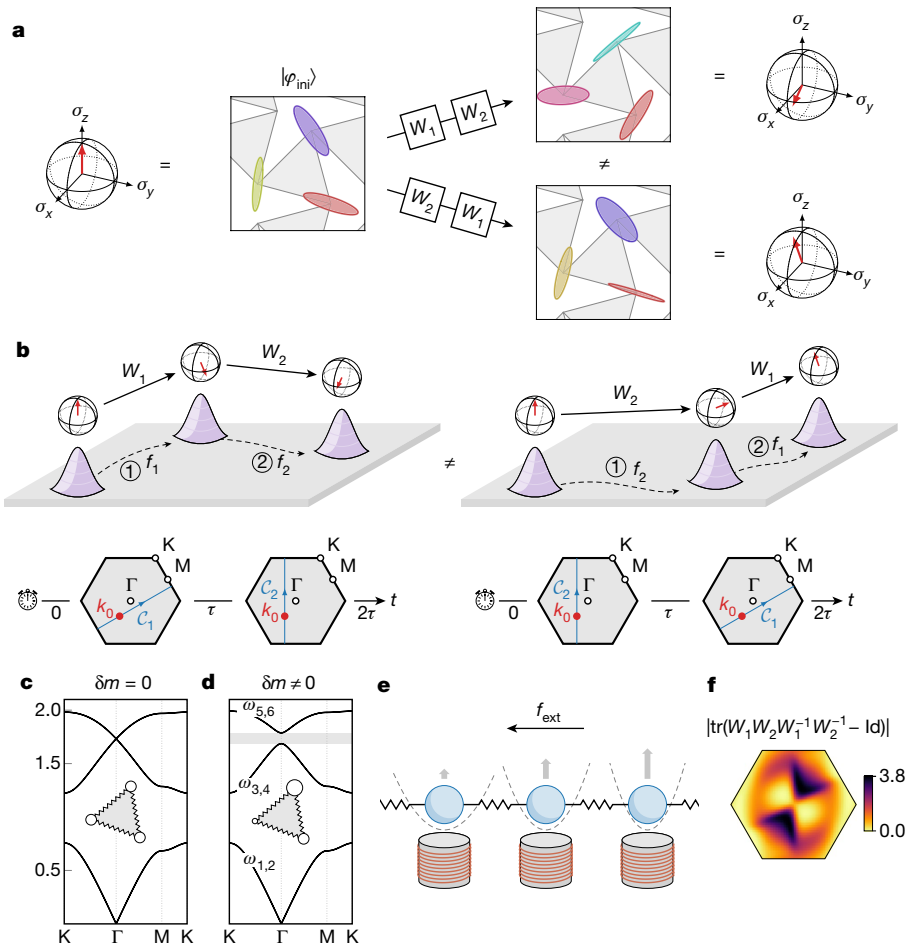

Fig. 4 | Mechanical spintronics via non-Abelian geometric phases. Pushing on a wavepacket with an effective force f makes it move in momentum space and changes its pseudo-spin state $|\varphi\rangle$. This is described by the holonomy W of a non-Abelian Berry connection, which acts on $|\varphi\rangle$ as a single-qubit gate. **a**, The vibrational states $W_2W_1|\varphi_{ini}\rangle$ ($W_1W_2|\varphi_{ini}\rangle$) obtained after the sequence of forces (f_1,f_2) (of (f_2,f_1)) were applied for a duration τ such that $f_i\tau = a_i$* are represented by ellipses describing the motion of the masses, with the colour representing their phases. They are equivalently represented on a Bloch sphere (see Supplementary Information for a definition of the momentum-dependent basis). **b**, Sketch of the real space and momentum space trajectories (see Supplementary Information for the numerically integrated solutions). **c**, **d**, To avoid non-adiabatic transitions, an asymmetry δm is introduced between the three masses in a unit cell $(m_1, m_2, m_3) = (1-\delta m, 1, 1+\delta m)$, illustrated by circles of different sizes. As a consequence, the double Dirac cone becomes massive, with a gap (in grey) proportional to δm at first order, while the global twofold degeneracy is preserved. **e**, An effective force f_{ext} acting on the wavepackets is produced by applying a spatially varying harmonic potential that essentially shifts the optical bands in frequency proportionally to the potential (see Supplementary Information). **f**, Comparing $W_1W_2W_1^{-1}W_2^{-1}$ to the identity matrix provides a quantitative measure of the non-commutativity. The absolute value of the trace of their difference is plotted as a function of the starting point k_0 of the protocol. In the numerical simulations, we have considered a wavepacket projected on the bands with dispersions $\omega_3(k) = \omega_4(k)$, and we have set $k_0 = (2, 1)$ and $\delta m = 0.1$ (see Supplementary Information for details on the numerical computation and orders of magnitude).

We now show how non-Abelian sound waves arise in our self-dual mechanical structures. Non-commuting (or equivalently non-Abelian) behaviour is pervasive in mechanics, from the moves of a Rubik's cube to the non-holonomic dynamics of rolling spheres and robotic arms. Here, we focus instead on a more subtle phenomenon: the non-commutative behaviour of the classical excitations (that is, sound waves) that propagate on top of a background configuration. Note that because our reasoning does not rely on a particular length scale, it should also apply to nanostructures with quantum phonons. The propagation of a wavepacket constructed out of vibrational modes can be affected by geometric (or Berry) phases. For a single isolated band, the Berry phases are complex numbers of modulus one that manifestly commute. To obtain non-Abelian Berry phases, a set of (at least) two degenerate bands is required. The geometric phases then become 2 × 2 unitary matrices that do not need to commute[18,19].

The self-dual kagome lattice is a suitable platform to realize non-Abelian sound because it has a global twofold-degenerate phonon spectrum, allowing us to realize a pseudo-spin mechanical degree of freedom $|\varphi\rangle$, represented by a Bloch sphere in Fig. 4a, b. To do so, we need to isolate a single twofold-degenerate band in the spectrum. This is done by assigning different values to the three masses in the unit cell to lift the threefold rotation symmetry of the lattice, creating a gap in the double Dirac cone at Γ (see Fig. 4c, d). This modification preserves the self-dual symmetry of equation (2), so the global twofold degeneracy persists regardless of the values of the masses. Consider an acoustic wavepacket constructed from the central set of twofold-degenerate bands with dispersions $\omega_3(k) = \omega_4(k)$, where dispersion relations $\omega_i(k)$ with $i = 1,\ldots,6$ are labelled with increasing frequencies (see Fig. 4d). As we apply external forces to the wavepacket as in Fig. 4b, it evolves within the twofold-degenerate subset of mechanical vibrations, as long as the external perturbation is small enough (see Supplementary Information

for orders of magnitudes). The wavepacket can then be treated as a particle-like object described by semiclassical equations of motion (see Supplementary Information and refs. [20,32–34]) that govern the evolution of its semiclassical position $r(t)$, momentum $k(t)$ and pseudo-spin (that is, polarization) $|\varphi(t)\rangle$.

When a constant force is applied to the wavepacket, its momentum $k(t)$ increases linearly in time while its pseudo-spin state changes from an initial value $|\varphi_{\mathrm{ini}}\rangle$ to $W[\mathcal{C}]|\varphi_{\mathrm{ini}}\rangle$ (this situation is analogous to Bloch oscillations in solid-state physics). Here $W[\mathcal{C}] = P\exp\left(-\int_{\mathcal{C}} A\right)$ is a Wilson line operator, the non-Abelian analogue of a Berry phase, that acts on $|\varphi\rangle$ as a single-qubit gate, and A is the non-Abelian Berry connection[18,19] describing the twofold-degenerate band (see Supplementary Information). An effective force acting on wavepackets is not equivalent to a force acting on the elements of the mechanical lattice. The effective force on the wavepackets can be obtained through an additional harmonic potential imposed to each mass with a spatially dependent stiffness, as illustrated in Fig. 4e. This effective force is applied for a duration τ chosen so that the momentum changes by exactly one reciprocal lattice vector a_i^*. As a consequence, $\mathcal{C}_i(\lambda) = k_0 + \lambda a_i^*$ is a closed loop starting and ending at k_0 (see Fig. 4b), and the Wilson loop $W_i = W[\mathcal{C}_i]$ is the holonomy of the Berry connection along $\mathcal{C}_i$.

Pictorially, pushing on the wavepacket changes its pseudo-spin state: this change is the holonomy $W[\mathcal{C}]$. Here, the point is that the holonomies do not commute: when one pushes on the wavepacket in different directions, the order of the pushes matters because the pseudo-spin state keeps track of what happened. This is represented in Fig. 4b. After the forces (f_1, f_2) are sequentially applied during the appropriate duration, the pseudo-spin of a wavepacket initially at k_0 changes from any initial state $|\varphi_{\mathrm{ini}}\rangle$ to $W_2W_1|\varphi_{\mathrm{ini}}\rangle$. The reversed sequence (f_2, f_1) produces a different final pseudo-spin state $W_1W_2|\varphi_{\mathrm{ini}}\rangle$, because the two Wilson loops typically do not commute:

$$W_1W_2 \neq W_2W_1 \tag{3}$$

These non-commuting mechanical responses share similarities with non-Abelian excitations such as anyons[35–38]. However, in the present study, non-commutativity arises from how independent wavepackets respond to external forces, whereas for anyons it is associated with the exchange (braiding) of these quasi-particles with each other. In Fig. 4f, we assess how the choice of the initial point k_0 affects the non-commutativity of $W_1(k_0)$ and $W_2(k_0)$ by quantifying the deviation of $W_1W_2W_1^{-1}W_2^{-1}$ from the identity matrix.

Our results raise the prospect of materials in which information is encoded and processed using non-Abelian mechanical excitations and can be seen as a first step towards an extension of phononics[39] including mechanical pseudo-spins, which we call mechanical spintronics. More broadly, our work illustrates the power of duality relations in mechanics and wave physics. The counterintuitive degeneracies of elastic moduli and phonon spectra at the self-dual point suggest that dualities and their breaking may play as crucial a role in the design of metamaterials as symmetries currently do.

Online content

Any methods, additional references, Nature Research reporting summaries, source data, extended data, supplementary information, acknowledgements, peer review information; details of author contributions and competing interests; and statements of data and code availability are available at https://doi.org/10.1038/s41586-020-1932-6.

1. Kramers, H. A. & Wannier, G. H. Statistics of the two-dimensional ferromagnet. *Part I. Phys. Rev.* **60**, 252–262 (1941).
2. Savit, R. Duality in field theory and statistical systems. *Rev. Mod. Phys.* **52**, 453–487 (1980).
3. Urade, Y., Nakata, Y., Nakanishi, T. & Kitano, M. Frequency-independent response of self-complementary checkerboard screens. *Phys. Rev. Lett.* **114**, 237401 (2015).
4. Senthil, T., Vishwanath, A., Balents, L., Sachdev, S. & Fisher, M. P. A. Deconfined quantum critical points. *Science* **303**, 1490–1494 (2004).
5. Louvet, T., Delplace, P., Fedorenko, A. A. & Carpentier, D. On the origin of minimal conductivity at a band crossing. *Phys. Rev. B* **92**, 155116 (2015).
6. Devetak, I. Triangle of dualities between quantum communication protocols. *Phys. Rev. Lett.* **97**, 140503 (2006).
7. Hull C. M. & Townsend, P. K. Unity of superstring dualities. *Nucl. Phys. B* **438**, 109–137 (1995).
8. Maldacena, J. The large-*N* limit of superconformal field theories and supergravity. *Int. J. Theor. Phys.* **38**, 1113–1133 (1999)
9. Guest, S. & Hutchinson, J. W. On the determinacy of repetitive structures. *J. Mech. Phys. Solids* **51**, 383–391 (2003).
10. Souslov, A., Liu, A. J. & Lubensky, T. C. Elasticity and response in nearly isostatic periodic lattices. *Phys. Rev. Lett.* **103**, 205503 (2009).
11. Sun, K., Souslov, A., Mao, X. & Lubensky, T. C. Surface phonons, elastic response, and conformal invariance in twisted kagome lattices. *Proc. Natl Acad. Sci. USA* **109**, 12369–12374 (2012).
12. Kane, C. L. & Lubensky, T. C. Topological boundary modes in isostatic lattices. *Nat. Phys.* **10**, 39–45 (2013).
13. Paulose, J., Gin-ge Chen, B. & Vitelli, V. Topological modes bound to dislocations in mechanical metamaterials. *Nat. Phys.* **11**, 153–156 (2015).
14. Rocklin, D. Z., Zhou, S., Sun, K. & Mao, X. Transformable topological mechanical metamaterials. *Nat. Commun.* **8**, 14201 (2017).
15. Ma, J., Zhou, D., Sun, K., Mao, X. & Gonella, S. Edge modes and asymmetric wave transport in topological lattices: experimental characterization at finite frequencies. *Phys. Rev. Lett.* **121**, 094301 (2018).
16. Kramers, H. A. Théorie générale de la rotation paramagnétique dans les cristaux. *Proc. K. Akad. Wet. C* **33**, 959–972 (1930).
17. Klein, M. J. On a degeneracy theorem of Kramers. *Am. J. Phys.* **20**, 65–71 (1952).
18. Berry, M. V. Quantal phase factors accompanying adiabatic changes. *Proc. R. Soc. A* **392**, 45–57 (1984).
19. Wilczek, F. & Zee, A. Appearance of gauge structure in simple dynamical systems. *Phys. Rev. Lett.* **52**, 2111–2114 (1984).
20. Xiao, D., Chang, M.-C. & Niu, Q. Berry phase effects on electronic properties. *Rev. Mod. Phys.* **82**, 1959–2007 (2010).
21. Zanardi, P. & Rasetti, M. Holonomic quantum computation. *Phys. Lett. A* **264**, 94–99 (1999).
22. Coleman, S. *Aspects of Symmetry* (Cambridge Univ. Press, 1985).
23. Khanikaev, A. B., Fleury, R., Hossein Mousavi, S. & Alù, A. Topologically robust sound propagation in an angular-momentum-biased graphene-like resonator lattice. *Nat. Commun.* **6**, 8260 (2015).
24. Süsstrunk, R. & Huber, S. D. Classification of topological phonons in linear mechanical metamaterials. *Proc. Natl Acad. Sci. USA* **113**, E4767–E4775 (2016).
25. Huber, S. D. Topological mechanics. *Nat. Phys.* **12**, 621–623 (2016).
26. Matlack, K. H., Serra-Garcia, M., Palermo, A., Huber, S. D. & Daraio, C. Designing perturbative metamaterials from discrete models. *Nat. Mater.* **17**, 323–328 (2018).
27. Fruchart, M. et al. Soft self-assembly of Weyl materials for light and sound. *Proc. Natl Acad. Sci. USA* **115**, E3655–E3664 (2018).
28. Ozawa, T. et al. Topological photonics. *Rev. Mod. Phys.* **91**, 015006 (2019).
29. Ningyuan, J., Owens, C., Sommer, A., Schuster, D. & Simon, J. Time- and site-resolved dynamics in a topological circuit. *Phys. Rev. X* **50**, 021031 (2015).
30. Albert, V. V., Glazman, L. I. & Jiang, L. Topological properties of linear circuit lattices. *Phys. Rev. Lett.* **114**, 173902 (2015).
31. Lee, C. H. et al. Topolectrical circuits. *Commun. Phys.* **1**, 39 (2018).
32. Culcer, D., Yao, Y. & Niu, Q. Coherent wave-packet evolution in coupled bands. *Phys. Rev. B* **72**, 085110 (2005).
33. Shindou, R. & Imura, K.-I. Noncommutative geometry and non-Abelian Berry phase in the wave-packet dynamics of Bloch electrons. *Nucl. Phys. B* **720**, 399–435 (2005).
34. Onoda, M., Murakami, S. & Nagaosa, N. Hall effect of light. *Phys. Rev. Lett.* **93**, 083901 (2004).
35. Stern, A. & Lindner, N. H. Topological quantum computation—from basic concepts to first experiments. *Science* **339**, 1179–1184 (2013).
36. Iadecola, T., Schuster, T. & Chamon, C. Non-Abelian braiding of light. *Phys. Rev. Lett.* **117**, 073901 (2016).
37. Barlas, Y. & Prodan, E. Topological braiding of Majorana-like modes in classical metamaterials. Preprint at https://arxiv.org/abs/1903.00463 (2019).
38. Liu, Y., Liu, Y. & Prodan, E. Braiding flux-tubes in topological quantum and classical lattice models from class-D. Preprint at https://arxiv.org/abs/1905.02457 (2019).
39. Li, N.et al. Phononics: manipulating heat flow with electronic analogs and beyond. *Rev. Mod. Phys.* **84**, 1045–1066 (2012).

Methods

Non-Abelian holonomies

Geometric phases[18,40–42] describe the residual influence of its environment on a subsystem considered in isolation. They typically arise when the system undergoes a slow cyclic change of its parameters. In this situation, the state of the system is transported over the parameter space to describe the evolution. The change in this state from before to after one cycle is a geometric phase factor. Formally, it is the holonomy of a connection along the closed loop travelled in parameter space: the connection provides a covariant derivative describing the parallel transport in the vector bundle of system states. The holonomies (geometric phase factors) are not necessarily mere $U(1)$ phases, but can be matrices referred to as non-Abelian geometric phases[19], because the formalism allows for non-commuting holonomies (phase factors). More precisely, let

$$W(\mathcal{C}) = \mathcal{P}\exp\left(-\int_{\mathcal{C}} A\right) \tag{4}$$

be the holonomy of the connection along the curve $\mathcal{C}$ in parameter space. Here, A is the connection form (see Supplementary Information for details), called a non-Abelian gauge field in the context of gauge theory[43]. The quantity $W(\mathcal{C})$ is also called a Wilson loop operator[44], and can be computed numerically (see Supplementary Information). We are interested in situations where two holonomies do not commute, that is, when $W(\mathcal{C}_1)W(\mathcal{C}_2) \neq W(\mathcal{C}_2)W(\mathcal{C}_1)$ for two closed loops $\mathcal{C}_i$ starting (and ending) at the same point.

In the main text, we consider the propagation of wavepackets in a lattice of coupled mechanical oscillators. In this situation, the restriction to a subsystem described in isolation consists in assuming that the wavepacket stays in a given (set of degenerate) phonon bands, ignoring the bands with higher or lower frequencies. The parameter space is momentum space (that is, the Brillouin torus): the quasi-classical momentum changes because a force is applied to the wavepacket, and effectively acts as an external parameter from the point of view of the wavepacket (see Supplementary Information and refs. [20,32–34,45–50]). We emphasize that although the wavepacket moves both in momentum space and in position space, the non-Abelian geometric phase factors discussed in the main text are related to the trajectory in momentum space (not position space).

Non-Abelian holonomies arise in various physical contexts. The most common situation corresponds to an abstract parameter space[51–54]. In the situation analysed in the main text, the relevant parameter space is momentum space. This is similar to situations arising in the study of artificial spin–orbit coupling and non-Abelian gauge fields in optics[46–56] and in ultracold atomic gases[57–61]. Non-Abelian holonomies can also arise with position space as the relevant parameter space, such as in the non-Abelian Aharonov–Bohm effect[43] recently predicted and reported in optics[62,63]. Again, similar phenomena arise in ultracold atomic gases[57–61]. In another context, (non-Abelian) anyons[35,64–69] can also be understood as (non-Abelian) holonomies[69–71]; where the relevant parameter space is essentially describing the positions of the excitations. Interestingly, similar situations where classical excitations can be braided around one another were reported in optics and mechanics[36–38,72].

A fascinating facet of non-Abelian holonomies is the possibility of harnessing them to realize holonomic computations[21]. This idea was developed with quantum computation in mind, but it can indeed also be applied to classical systems (and hence, classical computation). From this point of view, the non-Abelian holonomies described in the main text can be seen as single-qubit gates. This is not enough to realize any quantum computation, even with quantum degrees of freedom (phonons). For that, one would need two-qubit gates, which would require an interaction between the wavepackets ignored in our analysis. Nonetheless, a suitable design of the pattern generating the effective forces should allow the realization of simple classical operations on the mechanical pseudo-spins carried by the wavepackets that would enrich the growing toolbox of phononic systems[39,73].

Semiclassical equations and Bloch oscillations

In the main text, we consider a wavepacket centred at a position r and a momentum k. We assume that this wavepacket is composed of a narrow band of frequencies corresponding to the two degenerate bands with dispersions $\omega_3(k) = \omega_4(k)$ (the same analysis could be done on the upper bands $\omega_5(k) = \omega_6(k)$). Its composition in the corresponding two-dimensional space is summarized by a pseudo-spin (polarization) $|\varphi\rangle$. In the context of wave physics, semiclassical approximations provide an approximate particle-like description of a wavepacket localized in both physical space and momentum space. For instance, geometrical optics can be viewed as a short-wavelength approximation of Maxwell equations[74]. Here, the position r and momentum k and the pseudo-spin $|\varphi\rangle$ are promoted to the status of dynamical variables (called semiclassical variables) that evolve when the system is perturbed, for example when the wavepacket propagates in a non-uniform medium. The equations describing the semiclassical dynamics of the wavepacket in a (perturbed) spatially periodic structure can be systematically obtained from the underlying wave equations[20,32,33,75–79] (see also refs. [34,45–50] for application to classical waves). They read

$$\begin{aligned} \dot{r}^{\mu} &= \frac{\partial \Omega}{\partial k_{\mu}} + \mathrm{i}\langle F^{\mu\nu}\rangle_{\varphi}\,\dot{k}_{\nu} \\ \dot{k}_{\mu} &= -\frac{\partial V}{\partial r^{\mu}} \\ \dot{\varphi} &= -(\mathrm{i}\Omega(k) + \mathrm{i}V(r) + A^{\mu}\dot{k}_{\mu})\varphi \end{aligned} \tag{5}$$

where $\Omega(k) = \omega_3(k) = \omega_4(k)$ is the dispersion relation of the relevant degenerate bands, $V(r)$ is an external potential, and $A(k)$ and $F(k)$ are the matrix-valued non-Abelian Berry connection and curvature forms of the degenerate band[18,19,43] (see Supplementary Information for more details).

The case of a constant (uniform) force $f_0 = -\partial_r V$ considered in the main text describes so-called Bloch oscillations[80], a situation realized in semiconductor superlattices[81] and in optical lattices of cold atoms[82] that provides a powerful tomographic tool for Bloch states[83–88]. In this case, the momentum equation $\dot{k} = f_0$ can be integrated to $k(t) = k_0 + f_0 t$. The pseudo-spin can then formally be obtained up to a phase as a Wilson loop along the momentum space trajectory (see Supplementary Information for more details).

Fabrication of the kagome lattices in LEGO bricks

The LEGO bricks realization of the kagome lattice allows us to demonstrate its collapse mechanism. It is composed of LEGO Technic liftarms connected by pins (see Supplementary Fig. 15).

Each pin can be attached to at most four liftarms, at different heights $h_1,\ldots,h_4$; and in the kagome lattice, it must be attached to exactly four liftarms. As the liftarms are rigid, they should not be bent, so the two pins connected by a liftarm should be attached at the same height. Amusingly, this constraint is similar to the ice rule of the six-vertex model. A practical consequence is that the unit cell of the kagome lattice has to be enlarged in the LEGO bricks realization. In our design, the unit cell is doubled with respect to the original lattice in order for the vertices to satisfy the ice-like rule. It is composed of 12 'liftarms 1 × 6 thin' (LEGO part 32063) and six 'pins without friction ridges lengthwise' (3673).

The presence of edges induces additional (unwanted) zero-energy mechanisms besides the global Guest–Hutchinson mechanism. They are suppressed as much as possible with an additional structure that prevents local motions without preventing the global deformation of the system.

Data availability

No external data set was used during the current study.

Code availability

The code used to compute the band structures and the holonomies, to perform the group-theoretical analysis, to integrate the semiclassical equations of motion and to verify the duality relations is available on Zenodo at https://doi.org/10.5281/zenodo.3417426 under the 2-clause BSD licence.

40. Wilczek, F. & Shapere, A. *Geometric Phases in Physics* (World Scientific, 1989).
41. Chruściński, D. & Jamiołkowski, A. *Geometric Phases in Classical and Quantum Mechanics* (Birkhäuser Boston, 2004).
42. Cohen, E. et al. Geometric phase from Aharonov–Bohm to Pancharatnam–Berry and beyond. *Nat. Rev. Phys.* **1**, 437–449 (2019).
43. Wu, T. T. & Yang, C. N. Concept of nonintegrable phase factors and global formulation of gauge fields. *Phys. Rev. D* **12**, 3845–3857 (1975).
44. Wilson, K. G. Confinement of quarks. *Phys. Rev. D* **10**, 2445–2459 (1974).
45. Bliokh, K. Y. & Bliokh, Y. P. Modified geometrical optics of a smoothly inhomogeneous isotropic medium: the anisotropy, Berry phase, and the optical Magnus effect. *Phys. Rev. E* **70**, 026605 (2004).
46. Onoda, M., Murakami, S. & Nagaosa, N. Geometrical aspects in optical wave-packet dynamics. *Phys. Rev. E* **74**, 066610 (2006).
47. Bliokh, K. Y., Frolov D. Y. & Kravtsov Y. A. Non-Abelian evolution of electromagnetic waves in a weakly anisotropic inhomogeneous medium. *Phys. Rev. A* **75**, 053821 (2007).
48. Bliokh, K. Y. & Freilikher, V. D. Polarization transport of transverse acoustic waves: Berry phase and spin Hall effect of phonons. *Phys. Rev. B* **74**, 174302 (2006).
49. Mehrafarin, M. &Torabi, R. Geometric aspects of phonon polarization transport. *Phys. Lett. A* **373**, 2114–2116 (2009).
50. Torabi, R. & Mehrafarin M. Berry effect in acoustical polarization transport in phononic crystals. *JETP Lett*. **88**, 590–594 (2009).
51. Alden Mead, C. Molecular Kramers degeneracy and non-Abelian adiabatic phase factors. *Phys. Rev. Lett*. **59**, 161–164 (1987).
52. Zee, A. Non-Abelian gauge structure in nuclear quadrupole resonance. *Phys. Rev. A* **38**, 1–6 (1988).
53. Alden Mead, C. The geometric phase in molecular systems. *Rev. Mod. Phys*. **64**, 51–85 (1992).
54. Sugawa, S., Salces-Carcoba, F., Perry, A. R., Yue, Y. & Spielman, I. B. Second Chern number of a quantum-simulated non-Abelian Yang monopole. *Science* **360**, 1429–1434 (2018).
55. Bliokh, K. Y. Rodriguez-Fortuño, F. J. Nori, F. & Zayats, A. V. Spin–orbit interactions of light. *Nat. Photonics* **9**, 796–808 (2015).
56. Ma, L. B. et al. Spin–orbit coupling of light in asymmetric microcavities. *Nat. Commun*. **7**, 10983 (2016).
57. Dalibard, J., Gerbier, F., Juzeliūnas, G. & Öhberg, P. Artificial gauge potentials for neutral atoms. *Rev. Mod. Phys*. **83**, 1523–1543 (2011).
58. Goldman, N., Juzeliūnas, G., Öhberg, P. & Spielman, I. B. Light-induced gauge fields for ultracold atoms. *Rep. Prog. Phys*. **77**, 126401 (2014).
59. Wu, Z. et al. Realization of two-dimensional spin–orbit coupling for Bose–Einstein condensates. *Science* **354**, 83–88 (2016).
60. Huang, L. et al. Experimental realization of two-dimensional synthetic spin–orbit coupling in ultracold Fermi gases. *Nat. Phys*. **12**, 540–544 (2016).
61. Aidelsburger, M., Nascimbene, S. & Goldman, N. Artificial gauge fields in materials and engineered systems. *C. R. Phys*. **19**, 394–432 (2018).
62. Chen, Y. et al. Non-Abelian gauge field optics. *Nat. Commun*. **10**, 3125 (2019).
63. Yang, Y. et al. Synthesis and observation of non-Abelian gauge fields in real space. *Science* **365**, 1021–1025 (2019).
64. Leinaas, J. M. & Myrheim, J. On the theory of identical particles. *Nuovo Cimento B* **37**, 1–23 (1977).
65. Wilczek, F. Quantum mechanics of fractional-spin particles. *Phys. Rev. Lett*. **49**, 957–959 (1982).
66. Fröhlich, J. in *Nonperturbative Quantum Field Theory* (eds 't Hooft, G. et al.) 71–100 (Springer, 1988).
67. Wen, X. G. Non-Abelian statistics in the fractional quantum Hall states. *Phys. Rev. Lett*. **66**, 802–805 (1991).
68. Moore, G. & Read, N. Nonabelions in the fractional quantum Hall effect. *Nucl. Phys. B* **360**, 362–396 (1991).
69. Nayak, C., Simon, S. H., Stern, A., Freedman, M. & Das Sarma, S. Non-Abelian anyons and topological quantum computation. *Rev. Mod. Phys*. **80**, 1083–1159 (2008).
70. Arovas, D., Schrieffer, J. R. & Wilczek, F. Fractional statistics and the quantum Hall effect. *Phys. Rev. Lett*. **53**, 722–723 (1984).
71. Lahtinen, V. & Pachos, J. K. Non-Abelian statistics as a Berry phase in exactly solvable models. *New J. Phys*. **11**, 093027 (2009).
72. Noh, J. et al. Braiding photonic topological zero modes. Preprint at https://arxiv.org/abs/1907.03208 (2019).
73. Maldovan, M. Sound and heat revolutions in phononics. *Nature* **503**, 209–217 (2013).
74. Born, M. et al. *Principles of Optics* (Cambridge Univ. Press, 1999).
75. Karplus, R. & Luttinger, J. M. Hall effect in ferromagnetics. *Phys. Rev*. **95**, 1154–1160 (1954).
76. Chang, M.-C. & Niu, Q. Berry phase, hyperorbits, and the Hofstadter spectrum: semiclassical dynamics in magnetic Bloch bands. *Phys. Rev. B* **53**, 7010–7023 (1996).
77. Sundaram, G. & Niu, Q. Wave-packet dynamics in slowly perturbed crystals: gradient corrections and Berry-phase effects. *Phys. Rev. B* **59**, 14915–14925 (1999).
78. Panati, G., Spohn, H. & Teufel, S. Effective dynamics for Bloch electrons: Peierls substitution and beyond. *Commun. Math. Phys*. **242**, 547–578 (2003).
79. Chang, M.-C. & Niu, Q. Berry curvature, orbital moment, and effective quantum theory of electrons in electromagnetic fields. *J. Phys. Condens. Matter* **20**, 193202 (2008).
80. Zener, C. A theory of the electrical breakdown of solid dielectrics. *Proc. R. Soc. A* **145**, 523–529 (1934).
81. Mendez, E. E. & Bastard, G. Wannier–Stark ladders and Bloch oscillations in superlattices. *Phys. Today* **46**, 34–42 (1993).
82. Raizen, M., Salomon, C. & Niu, Q. New light on quantum transport. *Phys. Today* **50**, 30–34 (1997).
83. Price, H. M. & Cooper, N. R. Mapping the Berry curvature from semiclassical dynamics in optical lattices. *Phys. Rev. A* **85**, 033620 (2012).
84. Atala, M. et al. Direct measurement of the Zak phase in topological Bloch bands. *Nat. Phys*. **9**, 795–800 (2013).
85. Jotzu, G. et al. Experimental realization of the topological Haldane model with ultracold fermions. *Nature* **515**, 237–240 (2014).
86. Aidelsburger, M. et al. Measuring the Chern number of Hofstadter bands with ultracold bosonic atoms. *Nat. Phys*. **11**, 162–166 (2014).
87. Flaschner, N. et al. Experimental reconstruction of the Berry curvature in a Floquet Bloch band. *Science* **352**, 1091–1094 (2016).
88. Li, T. et al. Bloch state tomography using Wilson lines. *Science* **352**, 1094–1097 (2016).

Acknowledgements We thank B. Bradlyn, V. Cheianov, S. Huber, W. Irvine, P. Lidon, N. Mitchell, S. Ryu, C. Scheibner, D. Son, A. Souslov, P. Wiegmann and B. van Zuiden for discussions. V.V. was supported by the Complex Dynamics and Systems Program of the Army Research Office under grant no. W911NF-19-1-0268. M.F. was primarily supported by the Chicago MRSEC (US NSF grant DMR 1420709) through a Kadanoff–Rice postdoctoral fellowship and acknowledges partial support by the University of Chicago through a Big Ideas Generator (BIG) grant and the Netherlands Organization for Scientific Research (NWO/OCW) as part of the Frontiers of Nanoscience program. LEGO is a trademark of the LEGO Group of companies which does not sponsor, license or endorse its use in this work.

Author contributions M.F. and V.V. designed the research, performed the research, and wrote the paper. Y.Z. and M.F. fabricated the mechanical kagome lattices. All authors contributed to discussions and manuscript revision.

Competing interests The authors declare no competing interests.

Additional information
Supplementary information is available for this paper at https://doi.org/10.1038/s41586-020-1932-6.
Correspondence and requests for materials should be addressed to M.F. or V.V.
Peer review information *Nature* thanks Muamer Kadic, Ronny Thomale and the other, anonymous, reviewer(s) for their contribution to the peer review of this work.
Reprints and permissions information is available at http://www.nature.com/reprints.